REGION-BASED ACTIVE SURFACE MODELLING AND ALPHA MATTING FOR UNSUPERVISED TUMOUR SEGMENTATION IN PET

Ziming Zeng[1,2]*, Jue Wang*[3]*, Tony Shepherd*[4] *and Reyer Zwiggelaar*[2]

1. Information and Control Engineering Faculty, Shenyang Jianzhu University, Liaoning, China
2. Computer Science Department, Aberystwyth University, UK.
3. Adobe Systems, Seattle, USA.
4. Turku PET Center and Department of Oncology and Radiotherapy, Turku University Hospital, Finland.

ABSTRACT

This paper presents a combination of existing advanced methods to solve the partial volume segmentation problem. It uses region-based active surface modelling in a hierarchical scheme to eliminate segmentation errors, followed by an alpha matting step to further refine the segmentation. This method can have an interest in several applications in medical imaging. We have validated our method on real PET images of head-and-neck cancer patients as well as custom designed phantom PET images. Experiments show that our method can generate more accurate segmentation than existing approaches.

***Index Terms*—** PET, 3D Active Surface Modelling, Alpha Matting Modelling, Tumour Segmentation

1. INTRODUCTION

Positron emission tomography (PET) is widely used for tumour imaging in cancer diagnosis, staging, treatment evaluation and radiotherapy planning, which require accurate segmentation of the volume of interest (VOI). Segmentation of PET VOIs is commonly performed by a combination of manual delineation and intensity thresholding. Manual segmentation is time-consuming and highly variable. Intensity thresholding lies at the core of most fully- or semi-automatic VOI segmentation methods [1] but the choice of threshold is arbitrary and results are affected by tumour heterogeneity and the low spatial resolution and signal-to-noise ratio.

More advanced methods include the Poisson Gradient Vector Flow (PGVF) of Hsu et al. [2] for edge-based segmentation and the Markov Random Field Expectation Maximisation (MAP-MRF EM) labelling technique of Gribben et al. [3]. These methods consider both intensity and spatial characteristics of PET data, but operate on a slice-by-slice basis, which ignores the information of the whole 3D volume. Also, these methods are hindered by the limited spatial resolution and partial volume effects.

In this paper we propose a new VOI segmentation method for PET that addresses the limitations above. Our method employs a hierarchical approach which combines an improved region-based active surface modelling method and alpha matting.

2. IMAGE SEGMENTATION METHOD

Our hierarchical segmentation scheme consists of three steps, as shown in the system flow-chart in Fig. 2. This approach considers both global and local voxel information. In the first two steps, an improved 3D active surface modelling method is used to segment the VOIs in PET volumes. In the last step, a trimap which contains a definite foreground, a definite background and an unknow region is automatically generated and an alpha matting technique is used to refine the segmentation results.

2.1. Improved 3D Active Surface Modelling

In the 3D segmentation step, a region-based active surface model [4, 5] and a global convex segmentation model [6, 7] are used to obtain an energy function that can be minimized by convex optimization. Subsequently, the energy function is minimized along with the deformation of the surface using a Split Bregman technique [7]. As in [7], the energy function is formally defined as:

$$E(\phi, f_1, f_2) = \int \varepsilon_\epsilon^x(\phi, f_1(x), f_2(x))dx + v\int \mid \nabla H_\epsilon(\phi(x)) \mid dx + \mu P(\phi), \tag{1}$$

where ϕ denotes the surface of tumours, $P(\phi) = \int (1/2)(\mid \nabla\phi(x) \mid -1)^2 dx$ is the level set regularization term. The region-scalable energy function is defined as

$$\varepsilon_\epsilon^x(\phi, f_1(x), f_2(x)) = \sum_{i=1}^{2} \lambda_i \int K_\sigma(x-y) \mid f_i(x) - I(y) \mid^2 M_i(\phi(y))dy, \tag{2}$$

where the 3D Gaussian kernel function is given by $K_\sigma(u) = (1/(2\pi^{3/2}\sigma^3))e^{-|u|^2/2\sigma^2}$. Given the locality of the kernel

function, the effect on ε generated by I(y) is almost zero when y is far away from x. The local fitting energy ε is determined by the value of σ. In Eq. 2, $M_1(\phi) = H(\phi), M_2(\phi) = 1 - H(\phi)$. The Heaviside function H is usually approximated by a smooth function $H_\epsilon(x) = (1/2)\big[1+(2/\pi)arctan\,((x/\xi))\big]$. As the grey level of tumours can vary between volumes, we change this function to attract the active surface to the boundary of the target object:

$$H_\epsilon(x) = \frac{1}{2}\left[1 + \frac{2}{\pi}arctan\left(\frac{x-T}{\xi}\right)\right], \tag{3}$$

where T ($0 \leq T \leq 1$) is a normalized value which is considered as the tumour grey level threshold. ξ is a constant value.

According to the derivation by Li et al. [5], the optimal functions $f_1(x)$, $f_2(x)$ that minimize $E(\phi, f_1, f_2)$ are:

$$f_i(x) = \frac{K_\sigma(x) * [M_i(\phi(x))I(x)]}{K_\sigma(x) * M_i(\phi(x))}, i = 1, 2. \tag{4}$$

For fixed $f_1(x)$, $f_2(x)$, the function ϕ can be written as:

$$\frac{\partial \phi}{\partial t} = \delta(\phi)\big[(-\lambda_1 e_1 + \lambda_2 e_2) + div(\frac{\nabla \phi}{\mid \nabla \phi \mid})\big], \tag{5}$$

where δ is the derivative of H_ϵ. $e_i(x) = \int K_\sigma(y-x) \mid I(x) - f_i(y) \mid^2 dy, i = 1, 2$. The simplified flow represents the gradient descent for minimizing the energy:

$$E(\phi) = \mid \nabla \phi \mid_1 + \langle \phi \cdot r \rangle, \tag{6}$$

where $r = \lambda_1 e_1 - \lambda_2 e_2$. Yang et al. [7] restricted the solution to lie in a finite interval in order to transform the constrained optimization problem to an unconstrained one. In this work, we constrain ϕ as $0 \leq \phi \leq 1$, which can guarantee a unique global minimal. The global convex model can be written as $min_{0\leq\phi\leq1}E(\phi) = min_{0\leq\phi\leq1}(\mid \nabla\phi \mid_1 + \langle \phi \cdot r \rangle)$. In [7], the minimization problem was written as $min_{0\leq\phi\leq1}E(\phi) = min_{0\leq\phi\leq1}(\mid \nabla\phi \mid_g + \langle \phi \cdot r \rangle)$.

Yang et al. [7] used the Split Bregman algorithm to solve the global convex model. The Split Bregman algorithm for minimizing the above function can be summarized as follows:

1: while $\parallel \phi^{k+1} - \phi^k \parallel > \Psi$ do
2: Define $r^k = \lambda_1 e_1^k - \lambda_2 e_2^k$
3: $\phi^{k+1} = GS(r^k, \overrightarrow{d^k}, \overrightarrow{b^k}, \lambda)$
4: $\overrightarrow{d}^{k+1} = shrink_g(\overrightarrow{b^k} + \nabla\phi^{k+1}, 1/\lambda)$
5: $\overrightarrow{b}^{k+1} = \overrightarrow{b}^k + \nabla\phi^{k+1} - \overrightarrow{d}^{k+1}$
6: Find $\Omega^k = \big\{x : \phi^k(x) > \mu\big\}$
7: Update e_1^k and e_2^k
8: end while,

where $GS(r^k, \overrightarrow{d^k}, \overrightarrow{b^k}, \lambda)$ denotes the Gauss-Seidal iteration method, $\overrightarrow{b}$, $\overrightarrow{d}$ are auxiliary variables, k is the iteration number, $shrink_g$ is a shrinkage frame (see [7]), and Ω is the segmented region. When the optimal ϕ is found, we can find the tumour region $\Omega^k = \big\{x : \phi^k(x) > 0.5\big\}$. We use this improved region-based active surface modelling method to segment VOIs in the PET data.

2.2. Hierarchical Segmentation Scheme

In the first segmentation step, the significantly noisy images are discarded before 3D volume data is generated. We first extract a close surface area by using a low threshold as the initialize surface to segment the PET volume data. The threshold T in Eq. 3 is estimated by calculating the average of the maximum grey level values of some selected slices in the volume. Specifically, we first use a median filter to remove noise in PET images, then find the maximum grey level value for each slice. Subsequently, we select the slice which contains the maximum value. This slice will be utilised to be compared with its three left neighbouring slices (named left neighbouring window). If the difference between this slice and any of the slice in the left window is less than the threshold φ, move the current slice to its closest left slice and compare the slice with its corresponding left window. This propagation carries on until the difference is above the threshold φ. The same process is also imposed to the right side. The selected slices are propagated in this way. The threshold T in Eq. 3, which is normalized between 0 and 1, then can be estimated by calculating the average maximum grey level values of these selected slices. For robust segmentation, a reliability metric is used to remove false positive VOIs. Specifically, the 6-connected neighborhood voxels are labeled in the results. If the tumour only exists in one or two slices, then the corresponding 3D labelling will be removed from the results.

The second segmentation step tries to find the none-detected regions that are selected in the first step. Specifically, morphology is used to dilate each 3D VOI generated in the previous step. We then use the generated surface as the initial closed surface, and segment the VOIs again using the local grey level voxels. The threshold T in this step is estimated by computing the average grey level values of the voxels in each dilated VOIs.

2.3. Segmentation by Using Alpha Matting

Due to the partial volume effect and limited image resolution, the segmentation results generated by the first two steps are not accurate enough. To further improve the segmentation accuracy, we introduce an alpha matting method [8] into our segmentation pipeline. We observe that the blur boundary of a VOI is caused by the fact that the boundary pixels are a mixture of foreground tissue (tumours) and background tissue (normal tissue). Instead of generating binary segmentation labels, a alpha matting techniques can generate a fractional alpha values between 0 and 1 for these pixels, which can be viewed as accurate soft segmentation.

To use alpha matting, a trimap has to be generated at first, which separates the image into three regions: definite foreground F, definite background B, and the unknown region U, as shown in Fig. 2. Our system automatically generates this trimap. Specifically, we use morphology to erode the previous segmentation result with a circular structuring element

to obtain the foreground F (show in white), then the background B (show in black) can be generated by dilating the binary segmentation. The unknown area (show in grey) can be generated by using the combined results.

To solve the alpha matting problem, we use the approach proposed by Levin et al. [8]. Using this approach each single slice is modeled as $I_i = \alpha F_i + (1-\alpha)B_i$, where I is the observed image, F and B are foreground and background, and α is the transparency parameter. It can be rewritten as $\alpha_i = aI_i + b$, where $a = 1/(F-B)$, $b = -B/(F-B)$. Then the problem is converted to finding α, a and b to minimize the cost function $J(\alpha, a, b) = \sum_{j\in I}\left(\sum_{i\in w_j}(\alpha_i - a_j I_i - b_j)^2 + \varepsilon a_j^2\right)$, where w_j is a small window around pixel j. For $J(\alpha) = min_{a,b}J(\alpha, a, b)$, we have $J(\alpha) = \alpha^T L\alpha$, where

$$L_{i,j} = \sum_{k|(i,j)\in w_k}\left(\delta_{i,j} - \frac{1}{|w_k|}\left(1 + \frac{(I_i-\mu_k)(I_j-\mu_k)}{\frac{\varepsilon}{|w_k|}+\sigma_k^2}\right)\right). \quad (7)$$

In this Laplacian function, $\delta_{i,j}$ is the Kronecker delta, μ_k and σ^2 are the mean and variance of the intensities in the window w_k around k which is usually 3×3, and $|w_k|$ is the number of pixels in this window. The details of the energy minimization process can be found in [8]. Solving the matting problem leads to a soft segmentation of VOIs in PET images.

3. EXPERIMENTS

To evaluate our method, we use 2 PET images of head-and-neck cancer patients and 2 of a custom-built tumour phantom [9, 10]. All images were acquired using a hybrid PET/CT scanner (GE Discovery) and the metabolic tracer [^{18}F]FDG. For each phantom VOI, ground truth was derived by thresholding the CT images. In the case of patient tumours, ground-truth segmentations were estimated using manual delineation by three separate expert physicians based at the imaging site. Each expert delineated each of three patient tumours twice, and from the resulting 6 ground truth estimates we randomly select one as the ground truth. (physician1_run1(a1), physician2_run2(a2), physician1_run2(b1)) from the resulting 18 ground truth.)

The detailed segmentation process for the example of a patient tumour is shown in Fig. 2. The clinical data sets are $256\times 256\times 37$ voxels. In the first step, all the maximum grey level values are generated from the 37 slices in the volume. Subsequently, the selected slices from 2 to 15 are identified by using the proposed criteria ($\varphi = 0.12$), then the threshold T in Eq. 3 is automatically estimated as 0.916. In Eq. 2, the 3D Gaussian kernel σ is 3 and $\lambda_i = 10$. In Eq. 3, $\xi = 0.1$. In the Split Bregman algorithm, $\Psi = 10^{-6}$, $1 < k < 30$. The improved active surface modelling result is used to segment the image and four false positive labellings are automatically removed. In the second step, the threshold T is recalculated for each dilated VOI and two VOIs are segmented again.

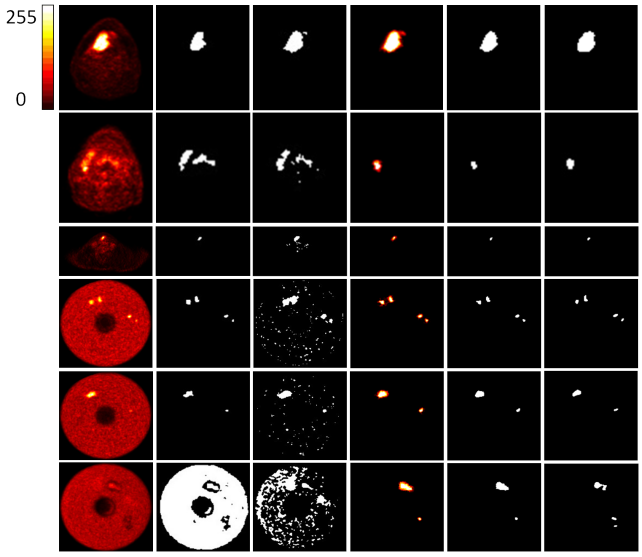

Fig. 1. Segmentation of the patient VOIs. From left to right: Color bar shown from 0 to 255, PET data (patient data (slice 28, slice 21 in patient A, and slice 9 in patient B), phantom data (slice 22, slice 26 in phantom C, and slice 21 in phantom D)), PGVF, MAP-MRF EM, our method, half thresholding results, ground truth.

We can see some none-detected regions are identified in this step. In the third step, the alpha matting algorithm is used to refine the segmentation on each slice. To compare against the ground truth which is a binary image, we threshold the soft segmentation generated by matting at half of the maximum grey level value for each slice, which leads to the final binary segmentation of VOIs.

Table 1. Dice index for tumour segmentation on PET data

Algorithm	PGVF [2]	MRF [3]	Our
Patient images	0.562	0.430	0.706
Phantom images	0.423	0.383	0.664
All images	0.493	0.407	0.685
Standard deviations	0.234	0.218	0.142

Fig. 1 shows a comparison with other methods on real and phantom PET data. Over-segmentation in the red region of the original image is apparent for the PGVF and MAP-MRF EM methods. This is partly explained by partial volume effects and the low spatial resolution of the images but could also be due to these slice-wise methods ignoring volumetric grey level information. For the phantom data, the MAP-MRF EM method does not perform well on images with significant noise. The PGVF method fails to segment the abnormal region, because the density of the abnormal region is similar to the surrounding tissue. In contrast, the developed method performs well with these images and provides accurate seg-

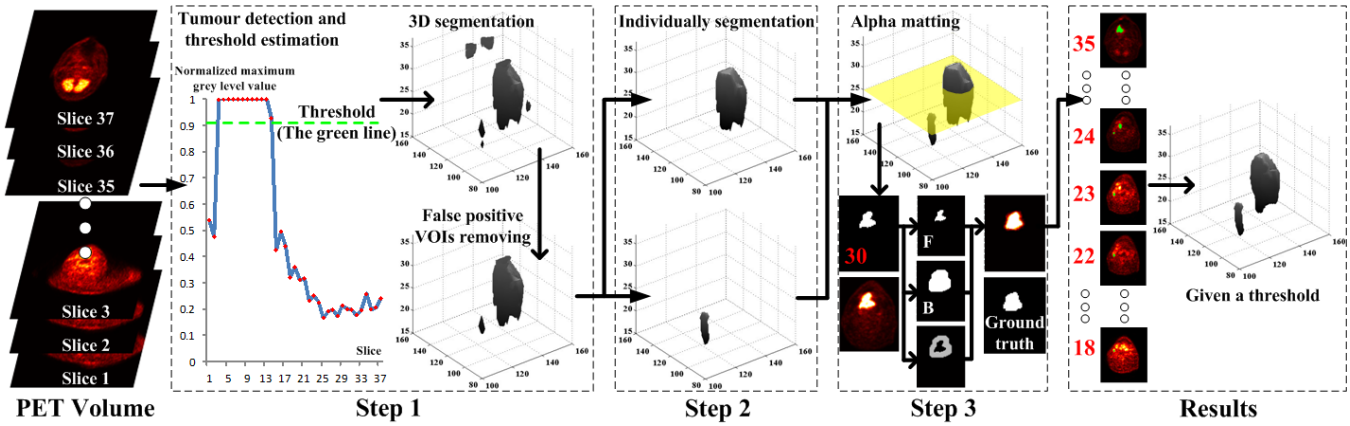

Fig. 2. Segmentation results of the hierarchical segmentation approach. The tumour is shown in green on each slice of the original volume. Tumour images are labeled with red color numbers

mentation results.

We evaluate segmentation accuracy in terms of overlap with ground-truth using the Dice similarity coefficient (DSC). We compare the DSC of our method and previous methods [2, 3]. Tab. 1 shows the mean DSC for real and phantom PET as well as the overall mean. Our results show improvements compared to previous methods.

4. CONCLUSIONS AND DISCUSSION

This paper presents a novel PET image segmentation scheme, based on an improved region-based active surface modelling method and alpha matting. Our method has the following advantages. First, the 3D voxel information is considered in a hierarchical scheme, which can largely eliminate segmentation errors. Second, the alpha matting technique is introduced to PET image segmentation for the first time, which can effectively deal with the partial volume effect problem. Finally, compared with previous approaches, our method is more robust for PET imaging segmentation. As future work, we will further evaluate our method on larger clinical datasets.

5. REFERENCES

[1] Y.E.Erdi, O.Mawlawi, S.M.Larson, M.Imbriaco, H.Yeung, R.Finn, and J.L.Humm, "Segmentation of lung lesion volume by adaptive positrone mission tomography image thresholding," *Cancer*, vol. 80, pp. 2505–2509, 1997.

[2] C.Hsu, C.Liu, and C.Chen, "Automatic segmentation of liver PET images," *Computerized Medical Imaging and Graphics*, vol. 32, pp. 601–610, 2008.

[3] H.Gribben, P.Miller, H.Wang, K.Carson, A.Hounsell, and A.Zatari, "Automated MAP-MRF EM labelling for volume determination in PET," ISBI, 2008.

[4] L.Wang, C.M.Li, Q.S.Sun, D.S.Xia, and C.Y.Kao, "Brain MR image segmentation using local and global intensity fitting active contours/surfaces," *Lecture Notes in Computer Science*, vol. 5241, pp. 384 – 392, 2008.

[5] C.Li, C.Kao, C.John, and Z.Ding, "Minimization of region-scalable fitting energy for image segmentation," *IEEE Trans. Image Processing*, vol. 17(10), pp. 1940–1949, 2008.

[6] T.F.Chan, S.Esedoglu, and M.Nikolova, "Algorithms for finding global minimizers of denoising and segmentation models," *SIAM Journal on Applied Mathematics*, vol. 66, pp. 1632–1648, 2006.

[7] Y.Yang, C.Li, C.Kao, and S.Osher, "Split Bregman method for minimization of region-scalable fitting energy for image segmentation," *Lecture Notes in Computer Science*, vol. 6454, pp. 117–128, 2010.

[8] A.Levin, D.Lischinski, and Y.Weiss, "A closed form solution to natural image matting," *Pattern Analysis and Machine Intelligence*, vol. 30, pp. 228–242, 2008.

[9] T.Shepherd, M.Teräs, and H.Sipilä, "New physical tumour phantom and data analysis technique exploiting hybrid imaging and partial volume effects for segmentation evaluation in radiation oncology," *European Journal of Nuclear Medicine and Molecular Imaging*, vol. 37(2), pp. S221, 2011.

[10] T.Shepherd, M.Teräs, and H.Sipilä, " Result of the contouring challenge, software session *II* at the *XII* Turku PET symposium, Turku PET centre, Finland," *[online]. Available: http://www.turkupetcentre.net / PET_symposium_XII_software_session/ Contouring ChallengeResults/.*